Acta of Bioengineering and Biomechanics
Vol. 25, No. 3, 2023

Original paper
DOI: 10.37190/ABB-02304-2023-01

The influence of Material Extrusion process parameters on the porosity and mechanical properties of PLA products for medical applications

MAŁGORZATA RUSIŃSKA[1], PIOTR GRUBER[1], GRZEGORZ ZIÓŁKOWSKI[1], MAGDALENA ŁABOWSKA[2], KAROLINA WILIŃSKA[2], PATRYCJA SZYMCZYK-ZIÓŁKOWSKA[1]*

[1] Center for Advanced Manufacturing Technologies – Fraunhofer Project Center, Faculty of Mechanical Engineering, Wrocław University of Science and Technology, Wrocław, Poland.
[2] Department of Mechanics, Materials and Biomedical Engineering, Faculty of Mechanical Engineering, Wrocław University of Science and Technology, Wrocław, Poland.

Purpose: The study addresses the growing need for personalized medicine and cost-effective manufacturing by investigating additive manufacturing (AM). It employs the Design of Experiments (DOE) to explore how fused filament fabrication (FFF) parameters affect porosity and mechanical properties of medical-grade polylactide (PLA) samples. *Methods*: Various PLA build configurations were fabricated and assessed using computed tomography (CT) scans for internal geometry and porosity. Compression tests were conducted to determine compressive strength, deformation, and Young's modulus. A comprehensive statistical analysis, utilizing three-way ANOVA, was carried out to establish the relationships between the process parameters and the obtained results. *Results*: The study reveals the impact of FFF process parameters (layer thickness, wall thickness, and infill density) on porosity and mechanical properties. Computed tomography analysis confirmed internal geometry and porosity, while compression tests provided insights into compressive strength, deformation, and Young's modulus. *Conclusions*: Optimal process parameters for desired mechanical properties and porosity in PLA models are highlighted, contributing to advanced medical applications. Informed FFF process parameter utilization enhances the potential for personalized therapeutic solutions and cost-effective pharmaceutical manufacturing.

Key words: *additive manufacturing, fused filament fabrication (FFF), polylactide (PLA), porosity, mechanical properties, medical applications*

1. Introduction

Interest in personalized medicine is constantly growing, as is the pharmaceutical companies' awareness in this area. Aiming to fulfill market requirements while maintaining cost-effective unit or individualized manufacturing, it is necessary to develop production processes with high flexibility, short manufacturing cycles and batches, achieving a viable cost per unit. Therefore, the pharmaceutical sector is exploring solutions to fabricate therapeutics with high potential to control the solubility and release rate of active substances, likewise the ability to dosage adjustment, intended for rapidly changing target users. Application of Additive Manufacturing (AM) technologies allows fulfilling these demands through the processing of material with a customized composition and the possibility to fabricate objects with arbitrary geometric forms affecting the dissolution time of the pharmaceutics [24], [28], [29].

Fused filament fabrication (FFF) is one of the most appreciated additive manufacturing technologies that

* Corresponding author: Patrycja Szymczyk-Ziółkowska, Faculty of Mechanical Engineering, Wrocław University of Science and Technology, ul. Łukasiewicza 5, 50-371 Wrocław, Poland, e-mail: patrycja.e.szymczyk@pwr.edu.pl
Received: August 31st, 2024
Accepted for publication: October 24th, 2024

has initiated the development of the 3D printer industry. According to ISO/ASTM 52900:2021(E), the technology is categorized as Material Extrusion, and more specifically as Material Extrusion with Thermal Reaction Bonding of polymers (MEX-TRB/P). The model is produced by layering a polymer material in the form of a filament. During the printing process, it is heated to achieve a semi-fluid state in the print head. The layers are placed on top of each other in the *XY* axes. When the printer finishes applying one layer, depending on the printer technology, the head rises or the base goes down by a specific distance called layer thickness. As the material is semi-fluid, the layers bond under appropriate temperature and quickly solidify into a uniform structure [8], [37]. This technology has found its applications in many sectors, including biomedical engineering due to the wide range of materials for prototyping. Increasing interest in transplantable organs, defects caused by diseases or surgical interventions, as well as risks resulting from transplantation (e.g., infections, graft rejection) have led to the development of the field allowing to obtain tissue scaffolds. Bone reconstruction structurally and functionally is still a significant challenge in regenerative medicine. To provide structural bone function, scaffolds are implanted in place of the tissue defect to initiate regeneration [4], [19]. Therefore, tissue scaffolds are intended to facilitate cell adhesion and migration [12], [31].

There are certain demands placed on the manufacture of scaffolds to accomplish their purpose. One of the most important requirements in scaffold fabrication is biocompatibility. The implanted material has to be accepted by the host organism, causing only a well-defined, organism-safe reaction [25], [27], [32]. Another key requirement is to ensure mechanical stability [32]. Additionally, scaffolds should have an appropriate porosity structure that is customized for their intended application ensuring that they are compatible with the host tissue and allowing for the ingrowth of new tissue and cell growth. Moreover, the material used for scaffold fabrication must be bioresorbable, thereby guaranteeing it to be completely removed from the recipient's body after defect regeneration [3], [4]. Scaffolds in tissue engineering are manufactured from a variety of materials such as metals, ceramics, polymers, carbon-based nanomaterials and composite materials [18], [36]. A promising material for medical applications, especially in tissue engineering where degradation is needed, is polylactide (PLA). It is a thermoplastic polymer that is completely biodegradable and bioresorbable. This compound is polymerized using lactic acid, obtained from starch and sugars, which are derived from renewable sources. PLA belongs to aliphatic polyesters and it is processed at about 190 °C. The glass transition temperature of polylactide is 55 °C while the melting point is 180 °C [2], [9], [15].

Although there have been numerous successful applications of conventionally manufactured scaffolds in clinical treatment, they exhibit several disadvantages. The foremost of these is the lack of accuracy of adjustment and the inflexibility of accommodation to specific conditions, which are individual features of the patient [35]. The success of AM techniques in medical engineering has made scaffold fabrication using this technology one of the most innovative surgical solutions in the last decade. This has been made possible by the ability to personalize treatment [1], [35].

The growing market of fused filament fabrication (FFF) technology users has a direct impact on the increase in demand for comprehensive information about the possibilities offered by this method, especially relating to the accuracy, repeatability, and quality of constructed parts. This knowledge can expand the target markets in which these manufacturing methods have not been used on a large scale so far. An emerging trend focused on conducting wide research is also visible in literature, examples can be found including research on commercially available materials [34], optimization (along with the development of a mathematical model) oriented to obtained geometric accuracy [22] as well as focusing on manufacturing time, material consumption and dynamic bending modulus [23]. Moreover, in the literature, studies regarding process parameters selection focus on the quality of manufactured parts are usually defined by the geometric accuracy of the digital model and surface quality. Examples include papers validating the influence of the dye in the PLA wire on the quality or material properties [23], [30], orientation in the workspace on the accuracy of the geometry and surface quality together with a method for their prediction [5] or the impact of process temperature and positioning on the work platform on the accuracy and repeatability [13]. There are also studies on the influence of the used slicing software, with the same process parameters, on the accuracy of the geometry reproduction [26]. In most of the articles, researchers examine the influence of parameters such as layer thickness, fill angle, number of layers, orientation in the workspace or on the platform, fill percentage or printhead temperature on mechanical properties, surface quality, accuracy, and repeatability of both dimensional and volumetric characteristics of parts.

2. Materials and methods

PLA material produced by Barrus Filaments (MCPP Netherlands BV, Netherlands) was used in this study. Polylactide acid was selected as one of the most popular and standard materials processed in FDM/FFF technology due to its good processing capabilities. It is characterized by low material shrinkage [16], relatively low processing temperature [10], and fine build plate adhesion. The cylindrical shape samples were manufactured on a self-built open-source FFF device (Fig. 1), dedicated to the fabrication of small objects, equipped with an E3D V6 printhead, supported by nozzle diameter of 0.25 mm (E3D-Online Limited, United Kingdom), not equipped with enclosed chamber. Constant process parameters used in research are summarized in Table 1.

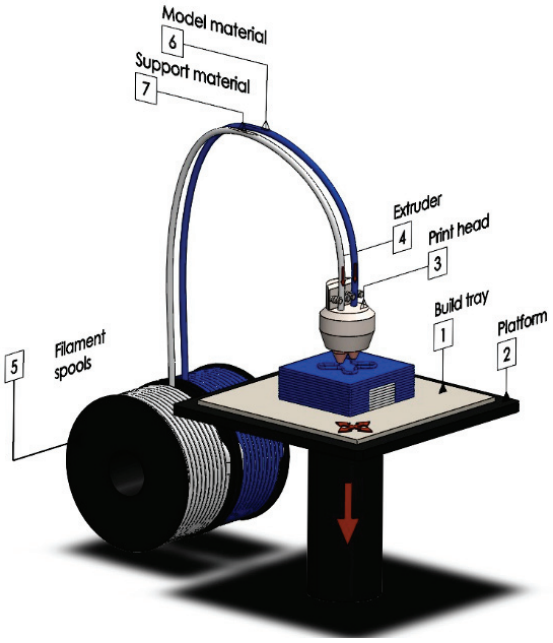

Fig. 1. Functional scheme of FFF technology [33]

Table 1. Constant FFF process parameters with hardware settings

Parameter		
Processing temperature	200	°C
Build plate temperature	60	°C
Nozzle diameter	0.25	mm
Printing speed	45	mm/s
Filament diameter	1.75	mm

The test specimen with a diameter of 5 mm and height of 10 mm were manufactured in *ZXY* (vertical) orientation (Table 2) and subsequently referred to as series (S1) to (S8). For each test series, 5 samples were prepared. Process data preparation was made using Cura 15.04.2 software (Ultimaker B.V., Netherlands).

Fused filament fabrication as an open-source technology has a series of parameters, which need to be set to properly prepare a manufacturing process. In Figure 2, the parameters are presented that have the greatest impact on the quality and properties of the manufactured part, including:

- layer thickness (A) – thickness of a single layer that is extruded during the FFF process, it depends on the material and nozzle diameter,
- wall thickness (B) – a result of the number of extruded contours and their overlapping, single path thickness depends mainly on the used nozzle diameter,
- model infill density (C) – a parameter calculated as the ratio of material extruded inside the model to its total volume (excluding a model's wall).

In the case of sample series with identical infill density and consistent sample dimensions, it is noteworthy that variations in sample series mass are primarily attributable to alterations in two other key process parameters: layer thickness and wall thickness. These variations have only a marginal impact on the final outcome for series S2, S4, S6, S8 where the biggest difference was 5.1 mg, but the impact for infill

Table 2. Summary of different build configurations examined during this study

	Dimensions of the sample			Build configurations		
Series	Diameter [mm]	Height [mm]	Mass [mg]	Layer thickness [mm]	Wall thickness [mm]	Infill density [%]
S1	4.89	10.05	137.20	0.1	0.5	25
S2	5.06	10.07	245.52	0.1	0.5	100
S3	4.92	10.05	187.80	0.1	1.0	25
S4	4.98	10.08	245.23	0.1	1.0	100
S5	4.95	10.07	139.35	0.15	0.5	25
S6	5.01	10.06	244.37	0.15	0.5	100
S7	4.98	10.06	188.37	0.15	1.0	25
S8	5.00	10.05	240.42	0.15	1.0	100

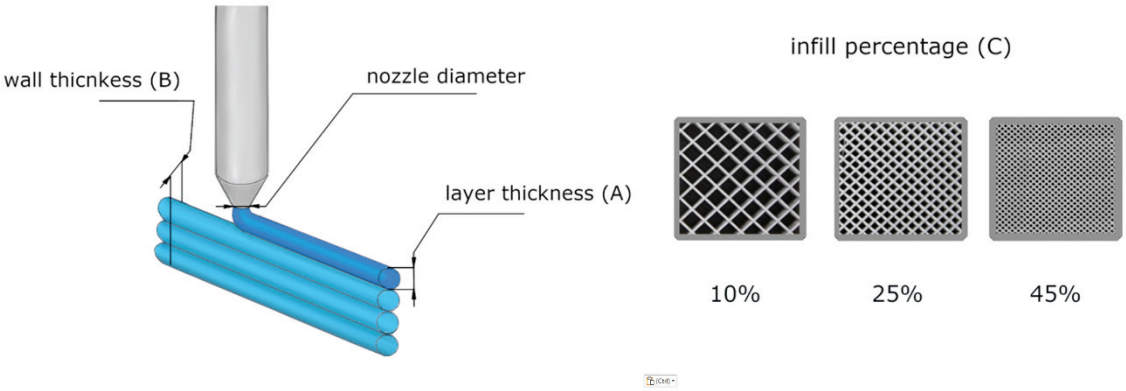

Fig. 2. Schematic representation of building parameters influenced properties of object manufactured by FFF

density on the level of 25% is drastically higher and is 51.17 mg with much lower general mass.

These three variable build parameters at two levels were considered for further investigation to evaluate their influence on sample porosity and mechanical properties. In order to determine the relationship between the geometry of the manufactured polymer scaffolds and the technological parameters used, a parametric model was developed. This model allowed for the theoretical calculation of the porosity of the test sample. The diameter of the tested sample, height, thickness of the outer wall of the model, and the model's infill density are taken into account. The formula for the theoretical porosity was presented in Eq. (1):

$$P_T = \frac{(d-2w_{th})^2(h-2w_{th})\left(1-\frac{I_{nf}}{100}\right)}{d^2 h}, \qquad (1)$$

where: d – diameter of a specimen, w_{th} – wall thickness, h – layer thickness, I_{nf} – infill density.

2.1. Porosity analysis

Technical computed tomography (CT) was used to obtain the internal geometry of the manufactured samples. The samples were scanned using the XCT system (Metrotom 1500, Carl Zeiss, Oberkochen, Germany). The system consists of a flat panel detector with a resolution of 1024 × 1024 px (400 µm pixel size) and 16-bit greyscale, a rotary table, and a microfocus X-ray tube with a maximum accelerating voltage of 225 kV and a maximum current of 1000 µA. To achieve the maximum resolution, the tube voltage was fixed at 140 kV and the current at 100 µA. The number of projections carried out during the 360° rotation of the sample was 1050 with 2 s integration time for each one. The data obtained were analyzed using the VG Studio MAX software (Volume Graphics GmbH, Heidelberg, Germany). The selected measurement parameters allowed to obtain the voxel size on the level 23.9 µm. The internal porosity, which determines the amount of porosity, was determined using the following Eq. (2):

$$P_R = \frac{V_{\text{por}}}{V_m + V_{\text{por}}} \cdot 100, \qquad (2)$$

where: V_{por} is the total volume of porosities, and V_m is the total volume of material.

2.2. Compression tests

Mechanical properties of additively manufactured specimens were carried out using the Instron 3384 testing machine (Instron, Norwood, MA, USA). The samples were preloaded with a force of 100 N. The traverse speed was constant at 2 mm/min. Before each series of measurements, the head was calibrated. The tests were conducted to the first decrease in the stress value corresponding to the first breakdown to determine the maximum stress values that the sample can transfer. Based on the obtained graphs, compressive strength, deformation, and Young's modulus for each type were calculated.

2.3. Statistical analysis

The fundamental purpose of research is to show the statistical significance of the impact of a selected factor on a variable of interest. Appropriate planning of the experiment enables one to adjust the parameters of multiple factors (inputs) systematically and identify which factors have the strongest influence on the final quality of the product (output). With the acquired knowledge, the parameters can be continuously im-

proved until optimal quality is achieved. Therefore, in this study, an experimental plan based on DOE factorial analysis 2k was undertaken. A two-level, full factorial experiment plan – 23 for the investigation of three parameters' influence on achieved process results is presented in Table 3.

Table 3. A two-level, full factorial design for three factors (2^3)

Full factorial analysis							
Series	A	B	C	AB	AC	ABC	Response
S1	1	1	1	1	1	1	y_1
S2	1	1	–1	1	–1	–1	y_2
S3	1	–1	1	–1	1	–1	y_3
S4	1	–1	–1	–1	–1	1	y_4
S5	–1	1	1	–1	–1	–1	y_5
S6	–1	1	–1	–1	1	1	y_6
S7	–1	–1	1	1	–1	1	y_7
S8	–1	–1	–1	1	1	–1	y_8

The statistical analysis aims to examine the correlation between observable variables. In this paper, three-way ANOVA was used in the analysis of the quality and mechanical properties. Statistical analysis in a three-way ANOVA enables a comparison of three groups of independent factors on the dependent variable. Layer thickness, wall thickness, and model infill density represent three independent variables. The response variables were porosity and compressive strength. The full-factorial design is shown in Table 4, while in Table 5, the breakdown of the ANOVA table used during this analysis is presented. For each case, five replicates were examined. The mathematical model for a two-level factorial experiment with three factors is as follows [21]:

$$Y_{ijkl} = \mu + \mathrm{A}_i + \mathrm{B}_j + \mathrm{C}_k + (\mathrm{AB})_{ij} + (\mathrm{AC})_{ik} + (\mathrm{BC})_{jk} + (\mathrm{ABC})_{ijk} + \varepsilon_{ijkl}, \quad \varepsilon \sim iidN(0,\sigma^2), \tag{3}$$

where: Y_{ijkl} is the response, μ is the overall mean, A_i is the factor effect of factor A, B_j is the factor effect of factor B, C_k is the factor effect of factor C, $(\mathrm{AB})_{ij}$ is associated with the interaction effect of factors A and B, $(\mathrm{AC})_{ik}$ is associated with interaction effect of factors A and C, $(\mathrm{ABC})_{ijk}$ is associated with interaction effect of factors A, B, and C, ε_{ijkl} is the random error, $\varepsilon \sim iid\ N(0,\ \sigma^2)$ is a restriction placed on the error term, meaning the error terms are independent and identically distributed. These error terms are distributed normally around a zero mean value and a variance of "σ^2".

Table 4. Summary of different build configurations studied during this study

Parameter	(–1) Levels (1)	
Layer thickness (A)	0.1	0.15
Wall thickness (B)	0.5	1.0
Infill density (C)	25	100

Table 5. Factorial experiment ANOVA table

Source of variation	Sum of squares (SS)	Degrees of freedom (DF)	Mean square (MS)	*F* ratio
Factor A	SSA	$a-1$	$\mathrm{MSA} = \frac{\mathrm{SSA}}{a-1}$	$\frac{\mathrm{MSA}}{\mathrm{MSE}}$
Factor B	SSB	$b-1$	$\mathrm{MSB} = \frac{\mathrm{SSB}}{b-1}$	$\frac{\mathrm{MSB}}{\mathrm{MSE}}$
Factor C	SSC	$c-1$	$\mathrm{MSC} = \frac{\mathrm{SSA}}{a-1}$	$\frac{\mathrm{MSC}}{\mathrm{MSE}}$
Interaction AB	SSAB	$(a-1)(b-1)$	$\mathrm{MSAB} = \frac{\mathrm{SSAB}}{(a-1)(b-1)}$	$\frac{\mathrm{MSAB}}{\mathrm{MSE}}$
Interaction AC	SSAC	$(a-1)(c-1)$	$\mathrm{MSAC} = \frac{\mathrm{SSAC}}{(a-1)(c-1)}$	$\frac{\mathrm{MSAC}}{\mathrm{MSE}}$
Interaction BC	SSBC	$(b-1)(c-1)$	$\mathrm{MSBC} = \frac{\mathrm{SSBC}}{(b-1)(c-1)}$	$\frac{\mathrm{MSBC}}{\mathrm{MSE}}$
Interaction ABC	SSABC	$(a-1)(b-1)(c-1)$	$\mathrm{MSABC} = \frac{\mathrm{SSABC}}{(a-1)(b-1)(c-1)}$	$\frac{\mathrm{MSABC}}{\mathrm{MSE}}$
Error	SSE	$abc(r-1)$	$\mathrm{MSE} = \frac{\mathrm{SSE}}{abc(r-1)}$	
Total	SST	$n_T - 1$		

3. Results

3.1. Porosity analysis

The tomographic analysis allowed for the evaluation of the inner and outer geometry of the manufactured scaffolds. Examples of the obtained results are shown in Fig. 3.

Based on the gathered data, the volume of the samples and the total porosity was determined. The results in correlation with process parameters sets are presented below in Tables 6 and 7.

The measured porosity did not exceed 5% for samples included in the series S2, S4, S6, and S8 manu-

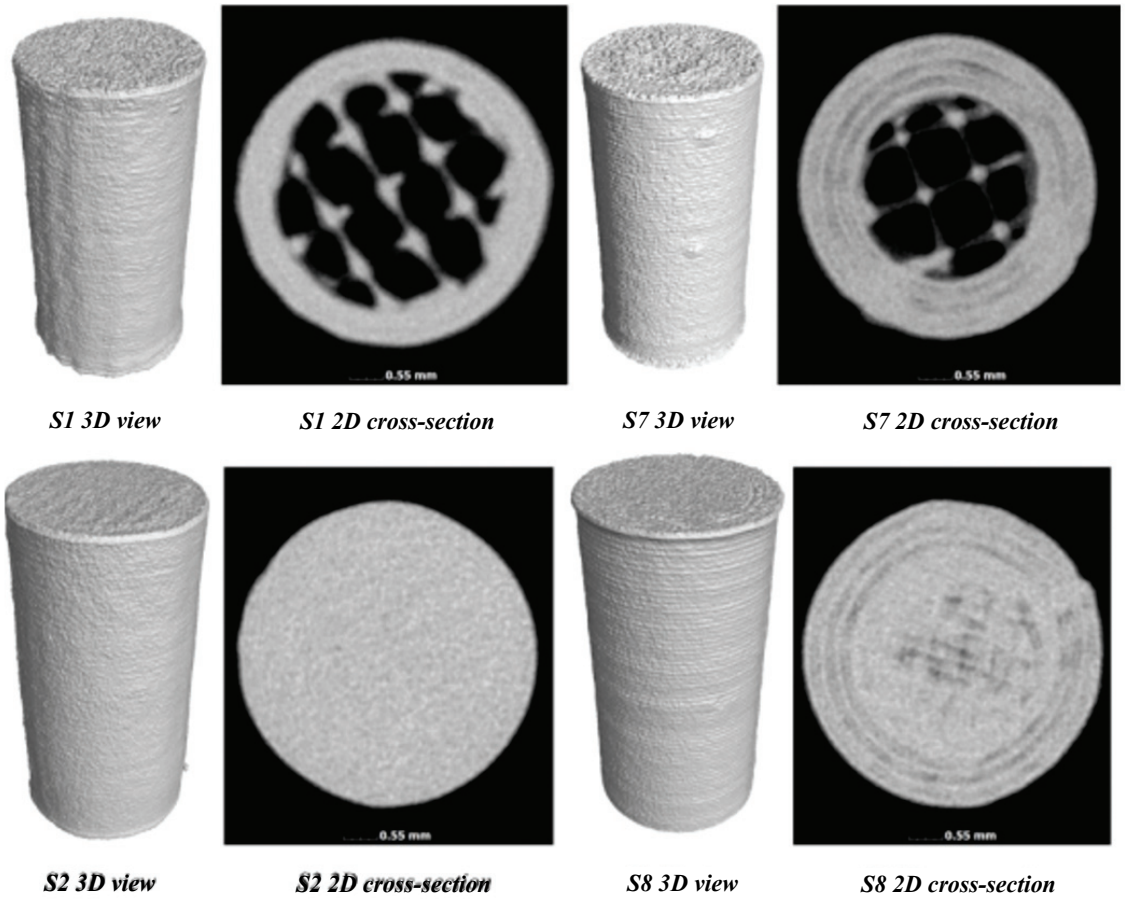

Fig. 3. The result of exemplary CT reconstructions 3D volumetric data and 2D projection

Table 6. Results of CT analysis of samples manufactured with different build configurations – porosity

Porosity [%]										
	Factors			Replications					Mean	Std.Dev.
Series	A	B	C	1	2	3	4	5		
S1	0.1	0.5	25	40.32	42.05	41.74	41.75	41.29	41.43	0.68
S2	0.1	0.5	100	1.17	0.94	1.10	1.03	1.08	1.06	0.09
S3	0.1	1.0	25	21.43	20.43	22.27	20.62	20.74	21.09	0.76
S4	0.1	1.0	100	0.75	0.62	0.77	0.59	0.66	0.68	0.08
S5	0.15	0.5	25	40.74	40.96	40.23	40.87	41.07	40.77	0.33
S6	0.15	0.5	100	2.53	2.41	2.83	2.90	2.66	2.67	0.20
S7	0.15	1.0	25	23.69	24.70	23.54	23.12	24.29	23.87	0.63
S8	0.15	1.0	100	3.75	3.55	4.94	4.85	3.96	4.21	0.64

Table 7. Results of CT analysis of samples manufactured with different build configurations – volume

Volume [mm^3]										
	Factors			Replications						
Series	A	B	C	1	2	3	4	5		
S1	0.1	0.5	25	111.36	108.45	108.93	109.00	110.67	109.68	1.26
S2	0.1	0.5	100	194.01	192.98	194.51	193.94	195.04	194.10	0.76
S3	0.1	1.0	25	147.77	150.06	147.37	149.43	149.02	148.73	1.13
S4	0.1	1.0	100	195.61	194.26	195.57	193.01	193.01	194.29	1.29
S5	0.15	0.5	25	110.73	109.41	111.90	111.17	110.21	110.68	0.94
S6	0.15	0.5	100	191.58	191.97	192.20	190.36	191.70	191.56	0.71
S7	0.15	1.0	25	145.23	143.41	146.27	145.17	143.72	144.76	1.18
S8	0.15	1.0	100	186.54	187.59	184.96	185.89	186.76	186.35	0.99

factured as a "solid" with an infill density at the level of 100% (Fig. 4).

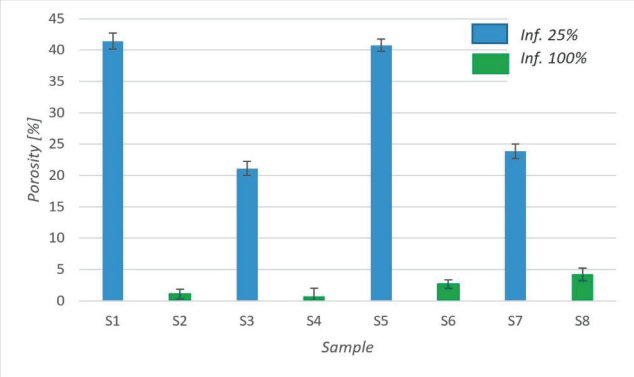

Fig. 4. The result of the porosity analysis ($N = 5$)

For a layer thickness of 0.1 mm, the difference between the theoretical and measured porosity did not exceed 2%, while for a layer thickness of 0.15 mm, the difference ranged from 2 to 4.5%. Based on the obtained results, it was revealed that layer thickness (A) has the greatest impact on the accuracy of the model produced (Fig. 5).

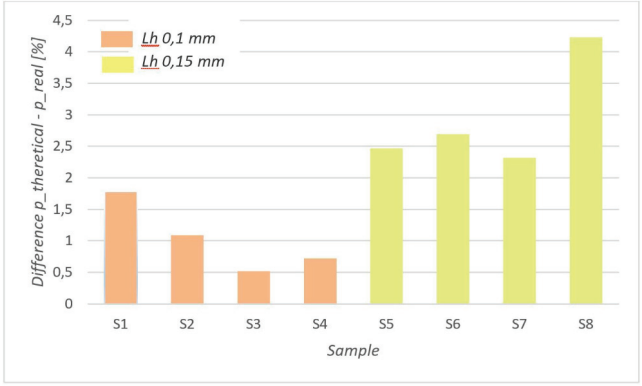

Fig. 5. The difference for theoretically determined porosity and the measured porosity

3.2. Compression tests

The results of the compression test are presented in Fig. 6, while the experimental data related to the process parameters are presented in Tables 8–10. It can be seen that the highest stress values were recorded for the samples S2, S4, S6, S8, i.e., those samples were manufactured with a filling factor equal to 100%. The introduction of porosity by reducing the

Table 8. Results of mechanical properties of samples manufactured with different build configurations – compression stress

Compression stress [MPa]										
	Factors			Replications						
Series	A	B	C	1	2	3	4	5		
S1	0.1	0.5	25	26.07	27.12	24.21	25.34	19.11	24.37	3.13
S2	0.1	0.5	100	58.59	62.39	63.52	64.57	68.17	63.50	3.09
S3	0.1	1.0	25	42.17	42.54	39.57	42.22	39.36	41.17	1.57
S4	0.1	1.0	100	66.88	69.47	46.17	66.36	66.65	63.11	9.55
S5	0.15	0.5	25	26.08	24.61	26.10	25.52	24.29	25.32	0.84
S6	0.15	0.5	100	59.75	61.89	60.75	60.04	59.54	60.39	0.95
S7	0.15	1.0	25	42.11	38.08	41.88	42.91	43.50	41.69	2.12
S8	0.15	1.0	100	61.62	61.93	59.99	60.82	58.47	60.57	1.39

Table 9. Results of mechanical properties of samples manufactured with different build configurations – Young's modulus

Young's modulus [MPa]										
	Factors			Replications					Mean	Std. Dev
Series	A	B	C	1	2	3	4	5		
S1	0.1	0.5	25	983.27	975.36	817.28	892.13	1085.54	950.72	101.34
S2	0.1	0.5	100	1883.69	1817.55	1879.70	1909.90	1942.21	1886.61	45.99
S3	0.1	1.0	25	1349.23	1391.09	1425.87	1378.15	1343.34	1377.54	33.51
S4	0.1	1.0	100	1995.24	1954.44	2433.23	1894.11	1887.43	2032.89	228.18
S5	0.15	0.5	25	915.74	819.74	791.68	879.40	742.72	829.86	68.89
S6	0.15	0.5	100	1730.79	1760.31	1677.92	1637.15	1627.66	1686.77	57.84
S7	0.15	1.0	25	1176.58	1200.70	1216.23	1258.59	1225.40	1215.50	30.37
S8	0.15	1.0	100	1824.36	1894.53	1860.78	1726.92	1629.55	1787.23	108.17

Table 10. Results of mechanical properties of samples manufactured with different build configurations – deformation

Deformation [%]										
	Factors			Replications					Mean	Std.Dev.
Series	A	B	C	1	2	3	4	5		
S1	0.1	0.5	25	13.90	16.11	14.22	14.98	13.73	14.59	0.98
S2	0.1	0.5	100	4.08	4.56	4.27	4.57	4.64	4.42	0.24
S3	0.1	1.0	25	28.95	27.82	20.19	27.53	19.23	24.74	4.64
S4	0.1	1.0	100	4.64	4.78	2.78	4.70	4.90	4.36	0.89
S5	0.15	0.5	25	20.03	20.72	22.93	18.50	22.41	20.83	1.96
S6	0.15	0.5	100	4.75	4.60	4.75	5.01	5.04	4.83	0.19
S7	0.15	1.0	25	35.89	23.03	30.25	34.82	41.70	33.14	6.97
S8	0.15	1.0	100	31.95	5.08	4.84	5.09	5.40	10.47	12.01

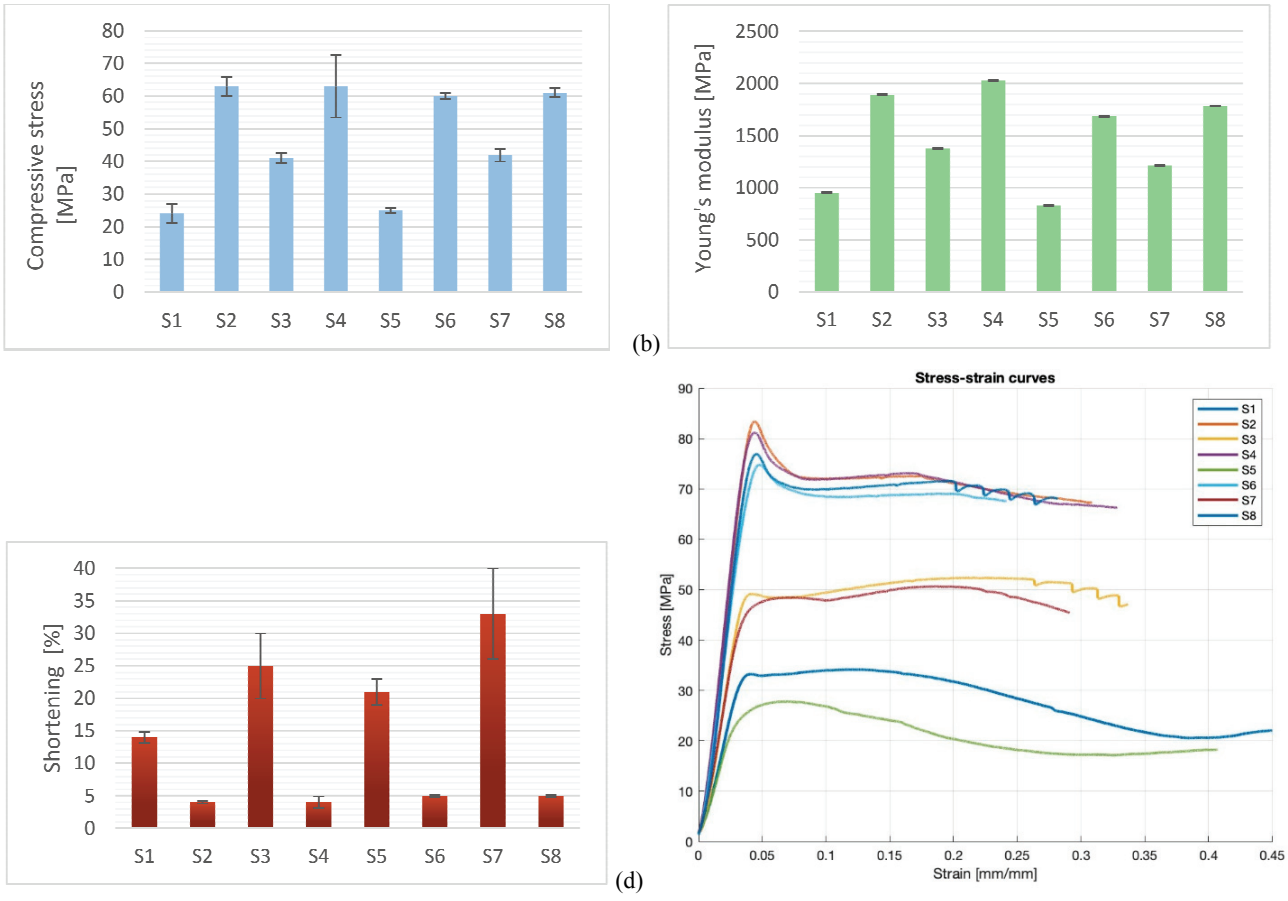

Fig. 6. Mechanical properties ($N = 5$): (a) compressive stress, (b) Young's modulus, (c) shortening, (d) stress–strain curves

infill density to the value of 25% for the samples with a wall thickness of 0.5 mm (S1 and S5) causes a reduction in compressive strength.

The deformation of samples changes depending on the compression stress parameters and Young's modulus (Fig. 6c). It can be observed that the deformation is the smallest for the samples S2, S4, S6, S8, i.e., those for which the highest values of Young's modulus were recorded, and thus showed the highest compressive stresses strength.

3.3. Statistical analysis

A three-way analysis of variance (ANOVA) was conducted using the experimental data presented in Tables 6 and 7 to determine which of the tested parameters resulted in the best mechanical properties. Statistical analyses were carried out with Statistica software (ver. 13, TIBCO Software Inc., California, CA, USA). The normal distribution of the obtained data was confirmed by the Shapiro–Wilk test (at a significance level of $p \geq 0.05$). Homogeneity of variance was verified by Brown–Forsythe test ($p \geq 0.05$). Determination of statistically significant differences ($p < 0.05$) between the research groups was conducted using a Tukey's honest significant difference (HSD) tests and the least squares (LS) means. Results from the ANOVA and treatment effects for the evaluated response variables are presented in Tables 11 to 14. During the study, eight null hypotheses (H0) regarding the treatment effects were considered and presented below:

1. $H_{0\ \text{total}}$: $\mu_{11} - \mu_{12} = ... = \mu_{mn}$ (equality testing of average treatment combinations)
   Reject H_0 if MST/MST > $F\ \alpha\ (abc - 1, abc(r - 1))$;
2. $H_{0\ \text{I}}$: $A_1 = A_2 = \ldots = A_I = 0$ (examines the differences between the layer thickness)
   Reject $H_{0\ \text{I}}$ if MSA/MSE > $F\ \alpha\ (a - 1, abc(r - 1))$;

Table 11. ANOVA results for porosity ($\alpha = 0.05$)

Source of variation	Degrees of freedom (DF)	Sum of squares (SS)	Mean square (MS)	*F* ratio
Model	1	11523.99	11523.99	<0.0001*
Error	32	7.99	0.25	
Total	33	11531.98		

* – the significance of parameter.

Table 12. ANOVA results for deformation ($\alpha = 0.05$)

Source of variation	Degrees of freedom (DF)	Sum of squares (SS)	Mean square (MS)	*F* ratio
Model	1	8611.88	8611.88	<0.0001*
Error	32	879.7	27.49	
Total	33	9491.58		

* – the significance of parameter.

Table 13. ANOVA results for Young's modulus ($\alpha = 0.05$)

Source of Variation	Degrees of Freedom (DF)	Sum of Squares (SS)	Mean Square (MS)	F Ratio
Model	1	86540431	86540431	<0.0001*
Error	32	345149	10786	
Total	33	86885580		

* – the significance of parameter.

Table 14. ANOVA results for compression stress ($\alpha = 0.05$)

Source of variation	Degrees of freedom (DF)	Sum of squares (SS)	Mean square (MS)	*F* ratio
Model	1	90284.2	90284.2	<0.0001*
Error	32	494.1	15.44	
Total	33	90778.3		

* – the significance of parameter.

3. $H_{0\,II}$: $B_1 = B_2 = \ldots = B_{II} = 0$ (examines the differences between the wall thickness)
   Reject $H_{0\,II}$ if MSB/MSE > $F\,\alpha\,(b-1, abc(r-1))$;
4. $H_{0\,III}$: $C_1 = C_2 = \ldots = C_{III} = 0$ (examines the differences between the infill density)
   Reject $H_{0\,III}$ if MSC/MSE > $F\,\alpha\,(c-1, abc(r-1))$;
5. $H_{0\,I*II}$: $(AB)_{ij} = 0$; i, j (tests for the presence of interaction between a and b)
   Rejected $H_{0\,I*II}$ if MSAB/MSE > $F\,\alpha\,((a-1)(b-1), abc(r-1))$;
6. $H_{0\,I*III}$: $(AC)_{ik} = 0$; i, k (tests for the presence of interaction between a and c)
   Rejected $H_{0\,I*III}$ if MSAC/MSE > $F\,\alpha\,((a-1)(c-1), abc(r-1))$;
7. $H_{0\,II*III}$: $(BC)_{jk} = 0$; j, k (tests for the presence of interaction between b and c)
   Rejected $H_{0\,II*III}$ if MSBC/MSE > $F\,\alpha\,((b-1)(c-1), abc(r-1))$;
8. $H_{0\,I*II*III}$: $(ABC)_{ijk} = 0$; i, j, k (tests for the presence of interaction between a, b, and c)
   Rejected $H_{0\,I*II*III}$ if MSABC/MSE > $F\,\alpha\,((a-1)(b-1)(c-1), abc(r-1))$.

In Tables 11 to 14, it can be seen that $p < 0.05$, indicates that there is a significant difference between the means of the treatment combinations. The hypothesis H_0 was rejected, and the model can be used to analyze the experimental data. Therefore, due to the significance of the model, the interactions between layer thickness, wall thickness, and infill density were examined. Tables 15 to 18 are compiled based on the treatment effect on porosity and mechanical properties for all variables.

The data listed in the effect matrix (Table 15) confirms the influence on porosity, that the interactions among all factors show significance, resulting in the rejection of the null hypotheses $H_{0\,I*II}$, $H_{0\,I*III}$, $H_{0\,II*III}$,

Table 15. Treatment effect table for porosity ($\alpha = 0.05$)

Source of variation	*N*	Sum of squares (SS)	Degrees of freedom (DF)	*F* ratio	*p*-value
A	5	32.83	1	131.48	<0.0001*
B	5	813.60	1	3258.0	<0.0001*
C	5	8784.11	1	35175.13	<0.0001*
AB	25	17.93	1	71.8	<0.0001*
AC	25	5.7	1	22.83	<0.0001*
BC	25	921.41	1	3689.69	<0.0001*
ABC	125	1.4	1	5.6	0.0241*

* – the significance of parameter.

Table 16. Treatment effect table for deformation ($\alpha = 0.05$)

Source of variation	*N*	Sum of squares (SS)	Degrees of freedom (DF)	*F* ratio	*p*-value
A	5	279.63	1	10.17	0.0031*
B	5	491.54	1	17.88	<0.0001*
C	5	2993.94	1	108.91	<0.0001*
AB	25	38.61	1	1.40	0.2447
AC	25	41.17	1	1.50	0.2299
BC	25	178.25	1	6.48	0.0159*
ABC	125	7.89	1	0.29	0.5959

* – the significance of parameter.

Table 17. Treatment effect table for Young's modulus ($\alpha = 0.05$)

Source of variation	N	Sum of squares (SS)	Degrees of freedom (DF)	*F* ratio	*p*-value
A	5	331606	1	30.74	<0.0001*
B	5	701198	1	65.01	<0.0001*
C	5	5699820	1	528.45	<0.0001*
AB	25	4730	1	0.44	0.5126
AC	25	16526	1	1.53	0.2248
BC	25	200026	1	18.55	<0.0001*
ABC	125	13	1	0.001	0.9720

* – the significance of parameter.

Table 18. Treatment effect table for compression stress ($\alpha = 0.05$)

Source of variation	*N*	Sum of squares (SS)	Degrees of freedom (DF)	*F* ratio	*p*-value
A	5	10.61	1	0.69	0.4133
B	5	680.96	1	44.10	<0.0001*
C	5	8259.30	1	534.91	<0.0001*
AB	25	0.00	1	0.00	0.9859
AC	25	31.22	1	2.02	0.1647
BC	25	695.06	1	45.02	<0.0001*
ABC	125	0.55	1	0.04	0.8512

* – the significance of parameter.

and $H_{0\ I*II*III}$. Table 16, for deformation, Table 17, for Young's modulus, and Table 18, for compression stress, have shown a significant difference in the interaction effect between factors B (wall thickness) and C (infill density) on the measured mechanical properties, respectively, resulting in the rejection of the hypothesis $H_{0\ II*III}$. The rest of the interactions between parameters do not indicate significance, therefore the assumed null hypotheses $H_{0\ I*II}$, $H_{0\ I*III,}$ and $H_{0\ I*II*III}$ fail to be rejected. The statistical analyses also indicate that the main factors (layer thickness, wall thickness, and infill density) have a significant effect on deformation (Table 16) and Young's modulus (Table 17), thus the null hypothesis $H_{0\ I}$, $H_{0\ II,}$ and $H_{0\ III}$ were rejected. In Table 18, it is shown that the effects of the main factors (wall thickness and infill density) have a significant influence on compression stress, resulting in the rejection of the null hypothesis $H_{0\ II}$ and $H_{0\ III}$. To

Table 19. Tukey honestly significant difference (HDS) for porosity ($\alpha = 0.05$)

	A level	B level	C level	Porosity LS mean
AB	0.1	0.5		21.25
AB		1		10.89
AB	0.15	0.5		21.72
AB		1		14.04
AC	0.1		25	31.26
AC			100	0.87
AC	0.15		25	32.32
AC			100	3.44
BC	0.1	0.5	25	41.10
BC		1	100	1.87
BC	0.15	0.5	25	22.48
BC		1	100	2.44
ABC	0.1	0.5	25	41.43
ABC			100	1.06
ABC		1	25	21.09
ABC			100	0.68
ABC	0.15	0.5	25	40.77
ABC			100	2.67
ABC		1	25	23.87
ABC			100	4.21

Table 20. Tukey honestly significant difference (HDS) for deformation ($\alpha = 0.05$)

	A level	B level	C level	Deformation LS mean
A	0.1			12.03
A	0.15			17.32
B		0.5		11.17
B		1		18.17
C			25	23.32
C			100	6.02
BC		0.5	25	17.71
BC		1	100	4.63
BC		0.5	25	28.94
BC		1	100	7.42

Table 21. Tukey honestly significant difference (HDS) for Young's modulus ($\alpha = 0.05$)

	A level	B level	C level	Young's modulus LS mean
A	0.1			1561.94
A	0.15			1379.84
B		0.5		1338.49
B		1		1603.29
C			25	1093.40
C			100	1848.37
BC		0.5	25	890.29
BC		1	100	1786.69
BC		0.5	25	1296.52
BC		1	100	1910.06

Table 22. Tukey honestly significant difference (HDS) for compression stress ($\alpha = 0.05$)

	B level	C level	Compression stress LS mean
B	0.5		43.38
B	1		51.64
C		25	33.14
C		100	61.88
BC	0.5	25	24.85
BC	1	100	61.92
BC	0.5	25	41.43
BC	1	100	61.83

examine factors that influence porosity and mechanical properties, Tukey's honest significant difference (HSD) tests (Tables 19–22) and the least squares (LS) means plots were performed (Figs. 7–14).

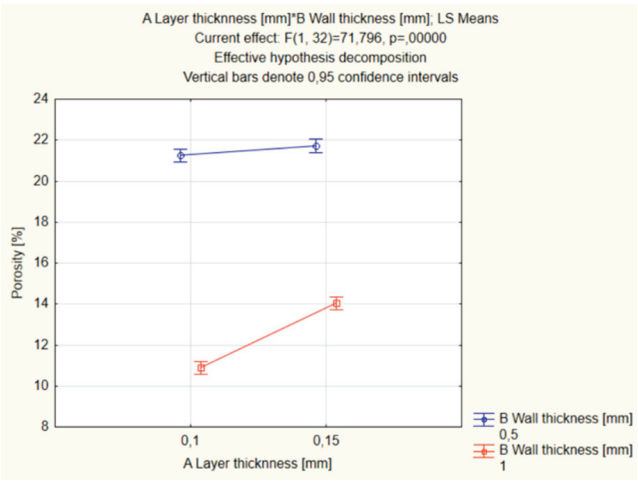

(a)

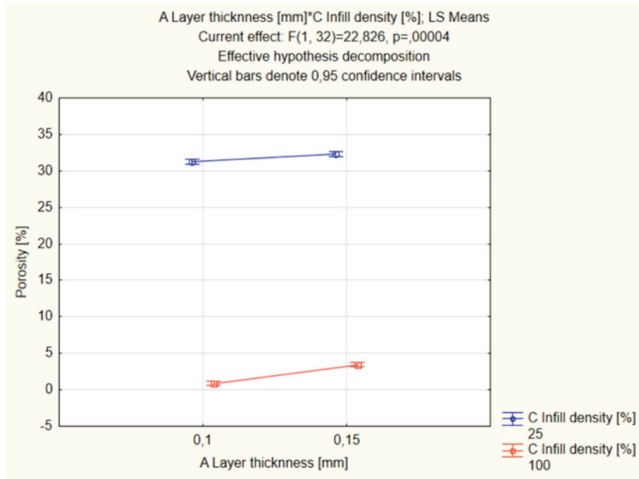

(b)

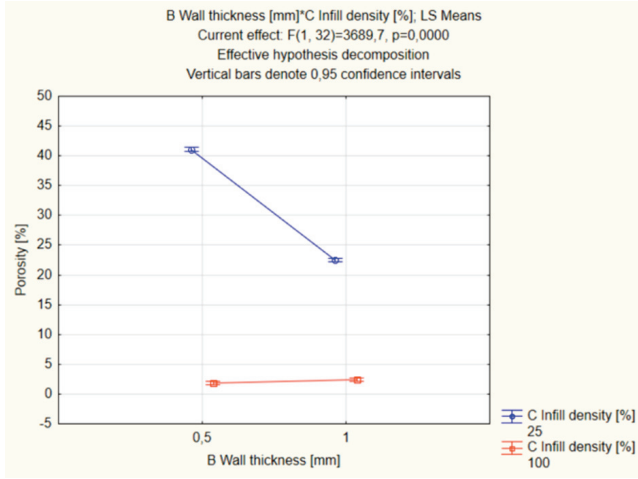

(c)

Fig. 7. Least square (LS) mean graph for interaction between two factors: (a) layer thickness – wall thickness, (b) layer thickness – infill density, c) wall thickness – infill density

The Tukey's test results (Table 20) and presented the least squares means plot (Figs. 9, 10) showed that the highest porosity is observed at 25% infill density and also for low levels of layer thickness (0.1 mm) and wall thickness (0.5 mm). However, the lowest porosity at a similar level was obtained for an infill density of 100% for all other parameters.

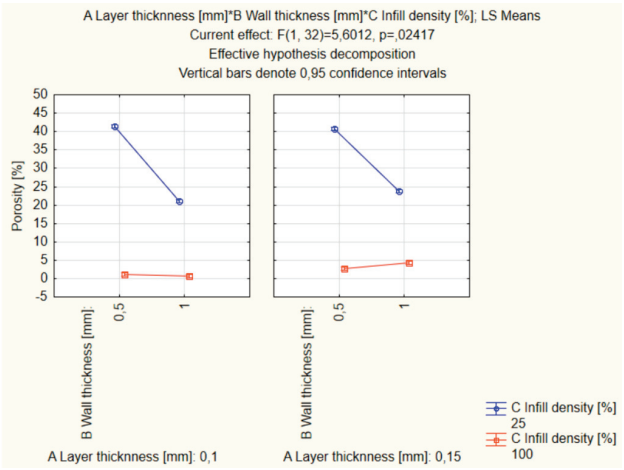

Fig. 8. Least square (LS) mean graph for three factors layer thickness, wall thickness, infill density

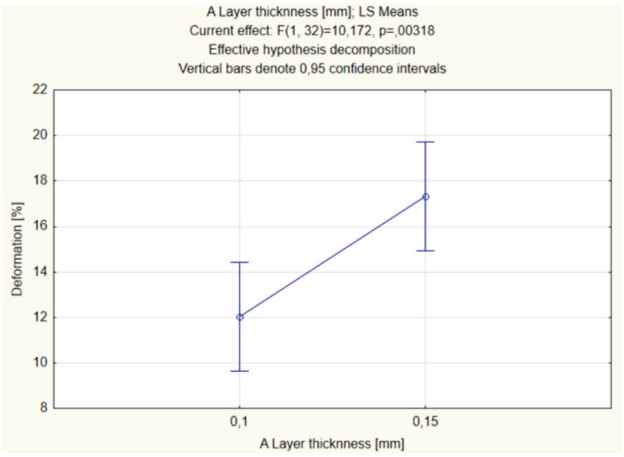

(a)

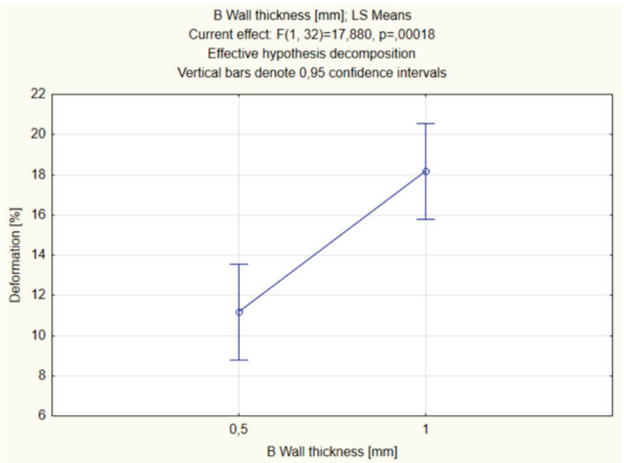

(b)

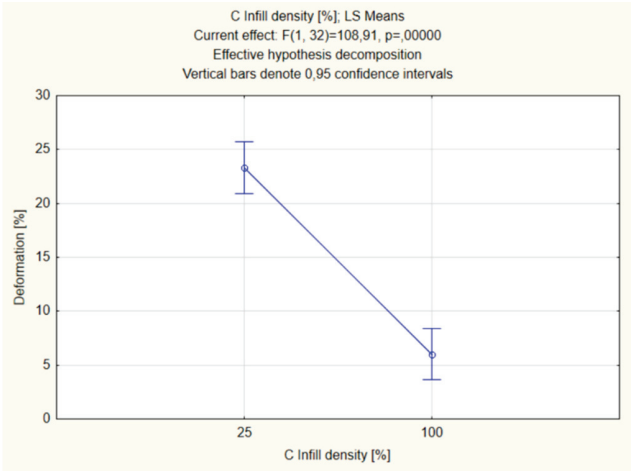

(c)

Fig. 9. Least square (LS) mean graph for three distinct factors: (a) layer thickness, (b) wall thickness, (c) infill density

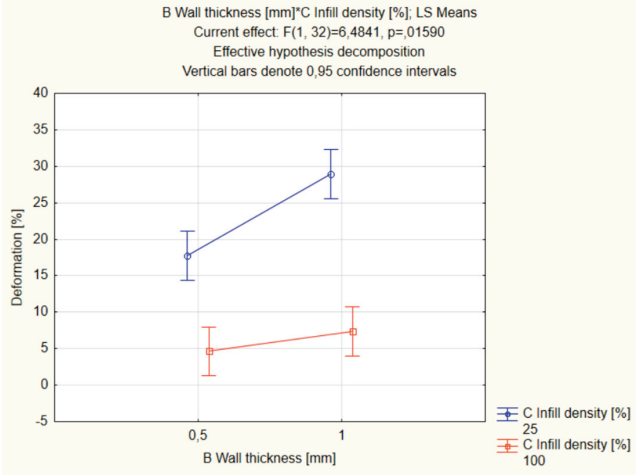

Fig. 10. Least square (LS) mean graph for two factors wall thickness and infill density

Table 21 containes Tukey's test results for the deformation of samples and Fig. 11 and Fig. 12 present the least square mean plot. The results show that the most significant effect on deformation is the level of infill percentage. The deformation decreases when the infill density is increased from 25 to 100%. The layer thickness and wall thickness also influence the degree of deformation because, for a higher value of these parameters, the degree of deformation increases.

In Table 22, Tukey's honestly significant difference (HDS) results are collected, and in Figs. 13, 14. the least square means for Young's modulus are presented, which reveals that for higher infill density higher Young's modulus values are achieved. For 25% and 100% infill density, Young's modulus is almost doubled. For individual main factors B and C, Young's modulus exhibits larger values of 0.1 mm for layer thickness and 1 mm for wall thickness, respectively.

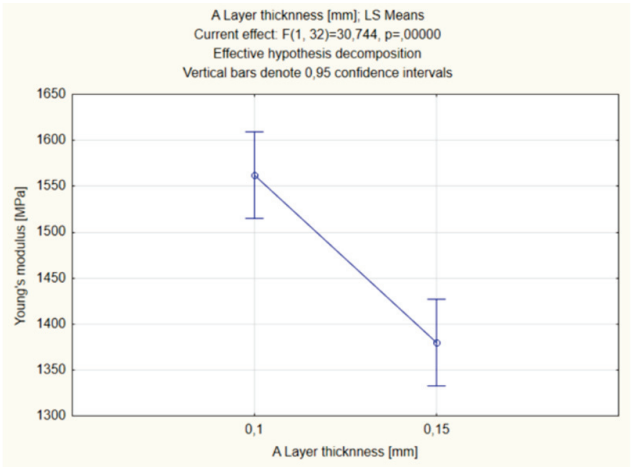

a)

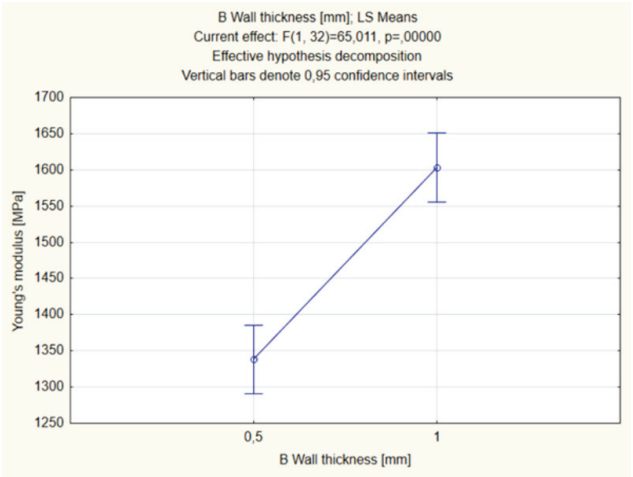

b)

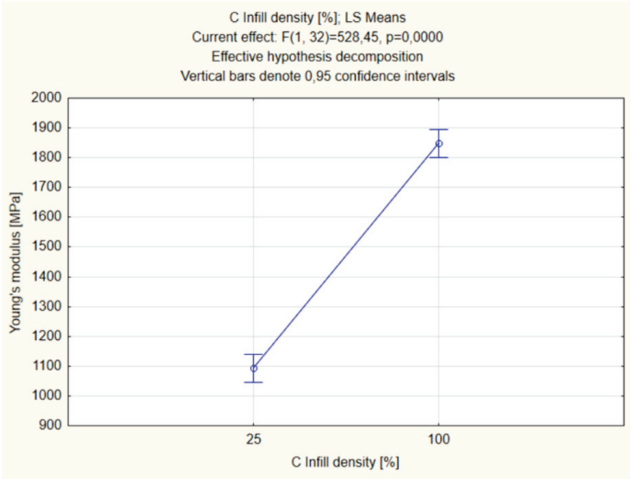

c)

Fig. 11. Least square (LS) mean graph for three distinct factors: (a) layer thickness, (b) wall thickness, (c) infill density

The final statistical analysis of compression stress considered the interaction between factors B and C, likewise the individual main factors B and C. According to data from Table 22, which contains the results of the Tukey test, and Figs. 13 and 14, it can be read that the

highest values of the compression test are achieved for 100% infill density and both levels of wall thickness (0.5 mm and 1 mm) at this infill density.

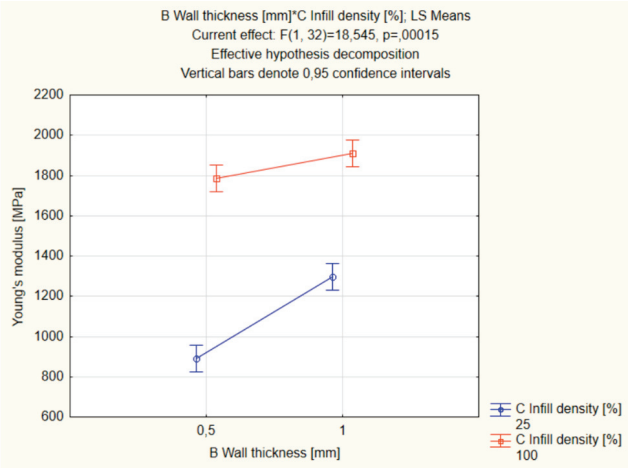

Fig. 12. Least square (LS) mean graph for two factors: wall thickness and infill density

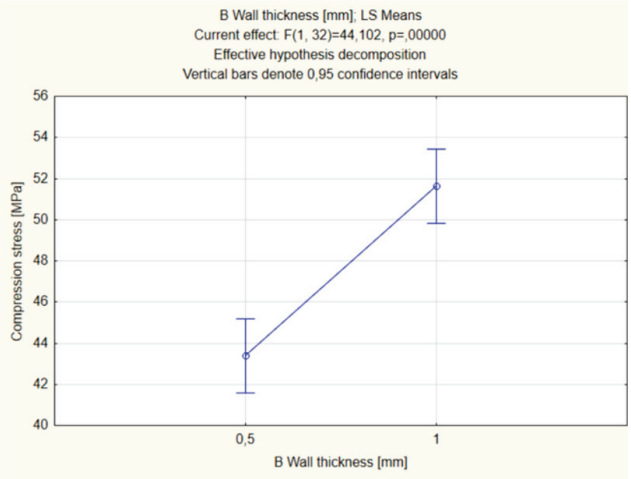

a)

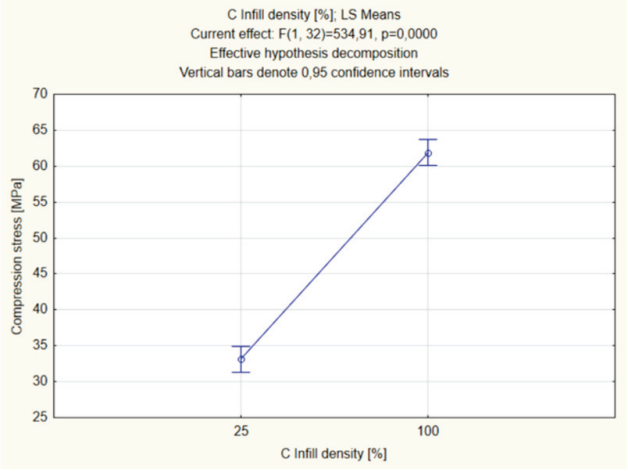

b)

Fig. 13. Least square (LS) mean graph for two distinct factors: a) wall thickness, b) infill density

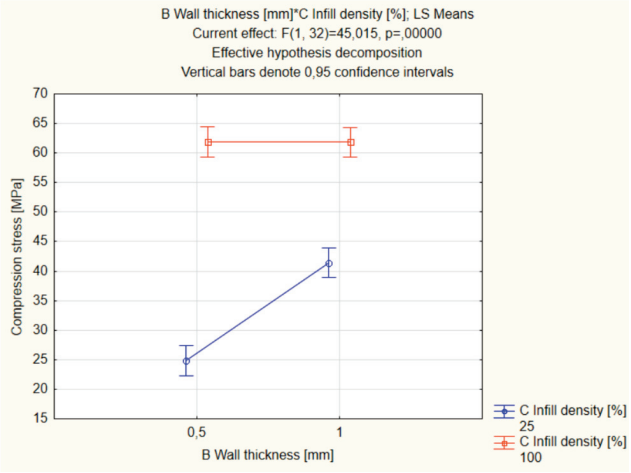

Fig. 14. Least square (LS) mean graph for three factors layer thickness, wall thickness, infill density

4. Discussion

Computed tomography is frequently used for the determination of the pore size and porosity degree of manufactured structures, but also for dimensional analysis or the evaluation of surface roughness [11], [17]. In the presented research the CT analysis has delivered data on the correlation between the process parameters and obtained porosity in final form of samples. It is clear that the samples manufactured as a "solid" (using 100% infill density) were characterized with maximum 5% porosity, and the difference between layer thickness parameter set on 0.1 mm or 0.15 mm, was between 2% and 4.5% of porosity, respectively. Indicating that this process parameter has the greatest impact on the accuracy of the model produced. Similar results are also found in the research conducted by other authors who have investigated the changing manufacturing parameters of PLA structures on porosity. An experiment carried out by Brackett et al. [6] demonstrated that the fabricated structures did not exceed 2% from the designated value, depending on the process parameters and infill degree. However, as shown in the studies undertaken by Majid and coworkers [20], the selection of a other material may significantly impact the difference in the resultant structural porosity. Researchers used acrylonitrile butadiene styrene (ABS) resulting in changes in porosity of up to 20–21%.

Another important aspect of additive manufacturing is the dependency of mechanical properties of final products and selected process parameters values. This research has conducted compression tests, and results were used to describe this correlation. The highest stress

values were recorded for the filling factor equal to 100% obtaining maximum of 63.50 MPa, when for the low infill value of 25% the maximal stress value was 41 MPa. Following this tendency the highest values of Young's modulus were recorded also for samples with 100% infill. Another important factor was the layer thickness parameter also causing drastic drop of 40 MPa in compressive strength when changed from 0.1 to 0.15 mm. The deformations observed were in compliance with highest compressive stress strength and Young's modulus. Similar observations were obtained by Gonabadi et al. [14] who evaluated the impact of process parameters (i.e., build orientation, infill density and infill patern) on the mechanical properties of PLA objects fabricated in FFF. The researchers observed that as the infill density increased, the tensile strength and Young's modulus also increased. The influence on the mechanical properties of the fabricated structures was also studied by Chacón et al. [7], where build orientation, layer thickness and flow rate were assesed. The evaluation of tensile and flexural strength revealed that a higher layer thickness generally resulted in increased strength.

In order to assess the impact of various parameters on characteristics of final samples and map the existing dependencies between used process parameters, the design of experiments plan was used, and the results of a three-way analysis of variance (ANOVA) were presented. The following key findings and conclusions can be drawn from the statistical analyses:

a) The porosity analysis (Table 15) results indicate that porosity is significantly influenced by all the tested parameters, including layer thickness, wall thickness, and infill density. Furthermore, the interactions between these factors were found to have a significant effect on porosity. It was observed that the highest porosity occurs when using 25% infill density, along with low levels of layer thickness (0.1 mm) and wall thickness (0.5 mm). Conversely, the lowest porosity was recorded when utilizing 100% infill density, irrespective of the other parameters. This suggests a strong correlation between infill density and porosity. Further analysis in this direction is necessary with a focus on more complex DOA plans where factors will be verified on three levels of variance. verifying whether the tested relationship is linear in the entire examined range.
b) The deformation analysis (Table 16) demonstrates that deformation is significantly affected by layer thickness, wall thickness, and infill density. Of these factors, the level of infill density emerged as the most significant influencer of deformation – with the drop of this parameter the occurred deformation increased. Additionally, it was noted that higher values of layer thickness and wall thickness lead to increased deformation.
c) The Young Modulus analysis reveal that Young's modulus is significantly influenced by layer thickness, wall thickness, and infill density. Among these parameters, the level of infill density exhibited the most substantial impact on Young's modulus. Conversely, other interactions between the parameters did not have a significant effect on Young's modulus.
d) Compression Stress analysis (Table 18) indicates that compression stress is significantly affected by wall thickness and infill density. The highest values of compression stress were achieved at 100% infill density, regardless of whether the wall thickness was 0.5 mm or 1 mm.

In summary, the study's statistical analyses reveal that the selected parameters, including layer thickness, wall thickness, and infill density, have a substantial impact on the mechanical properties of the material. These findings provide valuable insights for optimizing the material's properties based on specific application requirements. The interactions between these factors were also explored, and their significance was determined. The results of DoE plan has also allowed to construct regression model that will be used to predict the porosity based on selected values of process parameters within the tested ranges. These results contribute to a deeper understanding of the material's behavior and can guide future research and practical applications in various fields.

5. Conclusions

This paper aimed to evaluate the influence of factors such as layer thickness, wall thickness, and infill density on porosity, as well as the mechanical properties of parts fabricated with FFF. Porosity was measured using technical computed tomography (CT). Mechanical properties were measured using an Instron 3384 testing machine where compressive strength, deformation, and Young's modulus were investigated. It was found that the layer thickness had the greatest impact on the deformations generated in the tested models, with lower layer thickness resulting in less deformation. In the case of testing the effect of infill on deformation, it was shown that the smallest deformation is found with 100% infill. It was also proved that layer height and wall thickness have a significant effect on the mechanical properties of PLA models.

As for the infill, an almost double increase in Young's modulus value can be observed when it is increased from 25% to 100%. In addition, it can be found that porosity is the highest for 25% infill and lowest for 100%, with the same values of wall thickness (0.5 mm) and layer height (0.1 mm).

This study provides important insights into the influence of AM parameters on the mechanical properties and porosity of PLA models manufactured with FFF technology. Statistical analysis confirmed the significance of layer thickness, wall thickness, and infill density in determining the final properties of the fabricated parts. These results have practical implications for the optimization of 3D printing parameters to achieve desired mechanical properties and porosity in PLA models.

Acknowledgement

This work was supported by the National Centre for Research and Development in Poland (Grant No. LIDER/23/0098/L-9/17/NCBR/2018).

References

[1] ADEL I.M., ELMELIGY M.F., ELKASABGY N.A., *Conventional and recent trends of scaffolds fabrication: A superior mode for tissue engineering*, Pharmaceutics, 2022, 14, 306.

[2] BARAN E.H., YILDIRIM ERBIL H., *Surface modification of 3d printed pla objects by fused deposition modeling: A review*, Colloids and Interfaces, 2019, 3, 43.

[3] BAYART M., DUBUS M., CHARLON S., KERDJOUDJ H., BALEINE N., BENALI S., RAQUEZ J.M., SOULESTIN J., *Pellet-based fused filament fabrication (FFF)-derived process for the development of polylactic acid/hydroxyapatite scaffolds dedicated to bone regeneration*, Materials (Basel), 2022, 15, 5615.

[4] BODNÁROVÁ S., GROMOŠOVÁ S., HUDÁK R., ROSOCHA J., ŽIVČÁK J., PLŠÍKOVÁ J., VOJTKO M., TÓTH T., HARVANOVÁ D., IŽARIKOVÁ G., DANIŠOVIČ Ľ., *3D printed Polylactid Acid based porous scaffold for bone tissue engineering: an in vitro study*, Acta Bioeng. Biomech., Orig. Pap., 2019, 21.

[5] BOSCHETTO A., BOTTINI L., VENIALI F., *Integration of FDM surface quality modeling with process design*, Addit. Manuf., 2016, 12, Part B, 334–344.

[6] BRACKETT J., CAUTHEN D., CONDON J., SMITH T., GALLEGO N., KUNC V., DUTY C., *Characterizing the influence of print parameters on porosity and resulting density*, Solid Freeform Fabrication Symposium 2019.

[7] CHACÓN J.M., CAMINERO M.A., GARCÍA-PLAZA E., NÚÑEZ P.J., *Additive manufacturing of PLA structures using fused deposition modelling: Effect of process parameters on mechanical properties and their optimal selection*, Mater. Des., 2017, 124, 143–157.

[8] DEY A., EAGLE I.N.R., YODO N., *A review on filament materials for fused filament fabrication*, J. Manuf. Mater. Process, 2021, Vol. 5, Page 69, 2021, 5, 69.

[9] DONATE R., MONZÓN M., ALEMÁN-DOMÍNGUEZ M.E., *Additive manufacturing of PLA-based scaffolds intended for bone regeneration and strategies to improve their biological properties*, E-Polymers, 2020, 20, 571–599.

[10] DRUMMER D., CIFUENTES-CUÉLLAR S., RIETZEL D., *Suitability of PLA/TCP for fused deposition modeling*, Rapid Prototyp. J., 2012, 18, 500–507.

[11] DUPUY P.M., AUSTIN P., DELANEY G.W., SCHWARZ M.P., *Pore scale definition and computation from tomography data*, Comput. Phys. Commun., 2011, 182, 2249–2258.

[12] FICO D., RIZZO D., CASCIARO R., CORCIONE C.E., *A review of polymer-based materials for fused filament fabrication (FFF): Focus on sustainability and recycled materials*, Polymers (Basel), 2022, 14, 465.

[13] GAJDOS I., SLOTA J., *Influence of printing conditions on structure in FDM prototypes*, Tech. Vjesn., 2013, 20, 231–236.

[14] GONABADI H., YADAV A., BULL S.J., *The effect of processing parameters on the mechanical characteristics of PLA produced by a 3D FFF printer*, Int. J. Adv. Manuf. Technol., 2020, 111, 695–709.

[15] GRÉMARE A., GUDURIC V., BAREILLE R., HEROGUEZ V., LATOUR S., L'HEUREUX N., FRICAIN J.C., CATROS S., LE NIHOUANNEN D., *Characterization of printed PLA scaffolds for bone tissue engineering*, J. Biomed. Mater. Res. A, 2018, 106, 887–894.

[16] IBRAHIM M., HAFSA M.N., *Studies on rapid prototyping pattern using PLA material and FDM technique*, Appl. Mech. Mater., 2014, 465–466, 1070–1074.

[17] KHOSRAVANI M.R., REINICKE T., *On the use of X-ray computed tomography in assessment of 3D-printed components*, J. Nondestruct. Eval., 2020, 39.

[18] KRISHANI M., SHIN W.Y., SUHAIMI H., SAMBUDI N.S., *Development of scaffolds from bio-based natural materials for tissue regeneration applications: A review*, Gels, 2023, 9, 100.

[19] LIAO B., XU C., LI W., LU D., JIN Z.M., *Bionic mechanical design and SLM manufacture of porous Ti6Al4V scaffolds for load-bearing cancellous bone implants*, Acta Bioeng. Biomech., 2021, 23, 97–107.

[20] MAJID S.N.A., ALKAHARI M.R., RAMLI F.R., MAIDIN S., FAI T.C., SUDIN M.N., *Influence of integrated pressing during Fused Filament Fabrication on tensile strength and porosity*, J. Mech. Eng., 2017, SI 3, 185–197.

[21] MASSART D.L., VANDEGINSTE B.G.M., BUYDENS L.M.C., JONG S. DE, LEWI P.J., SMEYERS-VERBEKE J., *Two-level factorial designs*, Data Handling in Science and Technology, 1998, 659–682.

[22] MOHAMED O.A., MASOOD S.H., BHOWMIK J.L., *Optimization of fused deposition modeling process parameters for dimensional accuracy using I-optimality criterion*, Measurement, 2016, 81, 174–196.

[23] MOHAMED O.A., MASOOD S.H., BHOWMIK J.L., *Mathematical modeling and FDM process parameters optimization using response surface methodology based on Q-optimal design*, Appl. Math. Model., 2016, 40, 10052–10073.

[24] MOHAMMED A., ELSHAER A., SAREH P., ELSAYED M., HASSANIN H., *Additive manufacturing technologies for drug delivery applications*, Int. J. Pharm., 2020, 580, 119245.

[25] NIEMCZYK-SOCZYNSKA B., ZASZCZYŃSKA A., ZABIELSKI K., SAJKIEWICZ P., *Hydrogel, electrospun and composite materials for bone/cartilage and neural tissue engineering*, Materials (Basel), 2021, 14, 6899.

[26] OLEJARCZYK M., GRUBER K., ZIÓŁKOWSKI G., *Review of Available Software for Path Control of Personal 3D Printers Toolheads*, Tech. Issues, 2015, 3, 48–55.

[27] RANA D., ARULKUMAR S., VISHWAKARMA A., RAMALINGAM M., *Considerations on designing scaffold for tissue engineering*, [in:] A. Vishwakarma, P. Sharpe, S. Shi, M. Ramalingam (Eds.), *Stem Cell Biology and Tissue Engineering in Dental Sciences*, Elsevier Inc., 2015, 133–148.

[28] REDDY R.D.P., SHARMA V., *Additive manufacturing in drug delivery applications: A review*, Int. J. Pharm., 2020, 589, 119820.

[29] REINOSO M.R., CIVERA M., BURGIO V., BERGAMIN F., RUIZ O.G., PUGNO N.M., SURACE C., *3D printing and testing of rose thorns or limpet teeth inspired anchor device for tendon tissue repair*, Acta Bioeng. Biomech., 2021, 23, 63–74.

[30] SEARS F., *3D print quality in the context of PLA color*, Massachusetts Inst. Technol, 2016, 1–172.

[31] SINGH S., SINGH G., PRAKASH C., RAMAKRISHNA S., *Current status and future directions of fused filament fabrication*, J. Manuf. Process., 2020, 55, 288–306.

[32] SUAMTE L., TIRKEY A., BARMAN J., JAYASEKHAR BABU P., *Various manufacturing methods and ideal properties of scaffolds for tissue engineering applications*, Smart Mater. Manuf., 2023, 1, 100011.

[33] SZYMCZYK-ZIÓŁKOWSKA P., ŁABOWSKA M.B., DETYNA J., MICHALAK I., GRUBER P., *A review of fabrication polymer scaffolds for biomedical applications using additive manufacturing techniques*, Biocybern. Biomed. Eng., 2020, 40, 624–638.

[34] TANIKELLA N.G., WITTBRODT B., PEARCE J.M., *Tensile strength of commercial polymer materials for fused filament fabrication 3D printing*, Addit. Manuf., 2017, 15, 40–47.

[35] THAVORNYUTIKARN B., CHANTARAPANICH N., SITTHISERIPRATIP K., THOUAS G.A., CHEN Q., *Bone tissue engineering scaffolding: computer-aided scaffolding techniques*, Prog. Biomater., 2014, 3, 1–42.

[36] WOŹNA A.E., JUNKA A.F., SZYMCZYK P.E., *The influence of different composite mixtures (PLA/HA) manufactured with additive laser technology on the ability of S. aureus and P. aeruginosa to form biofilms*, Acta Bioeng. Biomech. Orig. Pap., 2018, 20, 101–106.

[37] YADAV A., ROHRU P., BABBAR A., KUMAR R., RANJAN N., CHOHAN J.S., KUMAR R., GUPTA M., *Fused filament fabrication: A state-of-the-art review of the technology, materials, properties and defects*, Int. J. Interact. Des. Manuf., 2022,